

**Measurement and comparison of distributional shift with applications to ecology,  
economics, and image analysis**

Kenneth J. Locey<sup>1\*</sup>, Brian D. Stein<sup>1</sup>

<sup>1</sup> Center for Quality, Safety and Value Analytics, Rush University Medical Center, Chicago, Illinois, 60612, USA.

\* Corresponding author. email: [Kenneth\\_J\\_Locey@rush.edu](mailto:Kenneth_J_Locey@rush.edu)

## Abstract

The concept of shift is often invoked to describe directional differences in statistical moments but has not yet been established as a property of individual distributions. In the present study, we define distributional shift (DS) as the concentration of frequencies towards the lowest discrete class and derive its measurement from the sum of cumulative frequencies. We use empirical datasets to demonstrate DS as an advantageous measure of ecological rarity and as a generalisable measure of poverty and scarcity. We then define relative distributional shift (RDS) as the difference in DS between distributions, yielding a uniquely signed (i.e., directional) measure. Using simulated random sampling, we show that RDS is closely related to measures of distance, divergence, intersection, and probabilistic scoring. We apply RDS to image analysis by demonstrating its performance in the detection of light events, changes in complex patterns, patterns within visual noise, and colour shifts. Altogether, DS is an intuitive statistical property that underpins a uniquely useful comparative measure.

**Keywords:** distribution shift; frequency distribution; histograms; image analysis; poverty measure; species rarity

## 1. Introduction

The concept of shift is often invoked to describe directional differences in average properties of, e.g., mass, time, temperature, distance, rates, and biometrics (White et al., 2006; Duffy et al., 2010; Sunday et al., 2015; Fink and Meyers, 2020; Hyam et al., 2023). Comparisons of frequency distributions also use the concept of shift to describe directional changes in variance, skewness, and kurtosis (Colles et al., 2016; Wan and Zhu, 2021; Suzuki et al., 2023). Others have gone beyond statistical moments to visualise distribution-wide shift via shift functions (Doksum, 1974; Rousselet et al., 2017). The terms data shift and distributional shift are also often used in machine learning to describe differences between training, validation, and testing data (Chen et al., 2022; Vadyala et al., 2022).

Despite its common use, the concept of shift has not yet been envisioned as a property of individual distributions. However, defining distributional shift (DS) as, e.g., the concentration of frequencies towards the lowest discrete class, may directly apply to economic studies wherein measures of poverty are invariably based on controversial and arbitrated poverty lines (Haughton and Khandker, 2009; Foster et al., 2010). The same concept could apply to ecological studies wherein measures of rarity are often based on arbitrary thresholds, e.g., the percent of species below a specific abundance (Magurran and McGill, 2010; Lynch and Neufeld, 2015). Though rarity is sometimes measured using skewness (Magurran and Henderson, 2003; Locey and Lennon, 2016), doing so conflates the asymmetry of a distribution with its concentration towards the lowest abundance class.

The concept of distributional shift as a global property of individual distributions has potential uses in the comparison of frequency distributions; specifically, in quantifying the direction and magnitude by which one distribution is shifted relative to another. Existing

statistical tools are not developed for this purpose. For example, shift functions are intended to visualise such differences but do not precisely quantify them (Doksum, 1974; Rousselet et al., 2017). While measures of distance, divergence, intersection, and probabilistic scoring are widely used to quantify differences between distributions, they do not indicate the direction of difference (Table 1) (Murphy, 1970; Deza and Deza, 2014; Szeliski, 2022). Though some statistical tests (e.g., Mann-Whitney U, one-sided two-sample Kolmogorov–Smirnov) can reveal the significance of one-tailed differences, thus indicating direction, their test statistics are rarely used as direct measures of difference (Gail and Green, 1976; Zar, 2009).

**Table 1.** Select measures used to compare frequency distributions.

Measure	Equation	Description
Chi-square Distance	$\frac{1}{2} \sum_{i=1}^k \frac{(f_{1i} - f_{2i})^2}{(f_{1i} + f_{2i})}$	One half the sum of squared differences between $k$ bins of two frequency distributions ( $f_1, f_2$ ) normalised by the sum of $f_{1i}$ and $f_{2i}$ (Asha <i>et al.</i> 2011).
Kolmogorov-Smirnov Distance	$\sup_x  F_1(x) - F_2(x) $	The maximum absolute difference between cumulative distribution functions (Deza and Deza 2014).
Kullback-Leibler Divergence	$\sum_{i=1}^k f_{1i} \log \left( \frac{f_{1i}}{f_{2i}} \right)$	Also known as relative information entropy. Measures the expected logarithmic difference in frequencies for corresponding bins, as the average information gain per observation needed to distinguish between $f_1$ and $f_2$ (Deza and Deza 2014).
Histogram Intersection	$\sum_{i=1}^k \min(f_{1i}, f_{2i})$	Measures the sum of the minimum values at each bin, emphasizing shared values in distributions (Deza and Deza 2014).
Earth Mover's Distance	$\min_{\gamma \in \Pi(P, Q)} \sum_{i,j} \gamma(i \cdot j) \cdot d(i, j)$	Measures dissimilarity between cumulative probability distributions by quantifying the minimum "work" required to transform one into another. The equation originates from optimal mass transportation (Deza and Deza 2014).
Ranked Probability Score	$\frac{1}{n} \sum_{i=1}^n \sum_{j=1}^k (F_{1ij} - F_{2ij})^2$	The squared differences between cumulative predicted frequencies and observed frequencies, normalised by the number of observations (Murphy 1970).

In the present work, we derive DS as the normalised sum of exponentiated cumulative frequencies, as calculated from discrete frequency distributions and histograms. Using a dataset of 44,090 samples of ecological communities, we demonstrate DS as a measure of species rarity. Using longitudinal data on family incomes and poverty, and international data on food commodities, we then demonstrate DS as a generalisable measure of poverty and scarcity. We then define relative distributional shift (RDS) as the difference in DS between distributions, yielding a signed (i.e., directional) measure. Using simulated random sampling we examine relationships of RDS to measures of distance, divergence, intersection, and probabilistic scoring, and explore how these relationships are influenced by binning and the shape of the population distribution. Focusing on the field of image analysis, we compare the performance of RDS to established measures in the detection light events, changes in complex patterns, patterns within visual noise, and shifts in the colour spectrum.

## **2. Distributional shift (DS)**

### ***2.1 Deriving a measure of DS***

A discrete frequency distribution,  $f$ , having  $n > 1$  observations distributed across  $k > 1$  discrete classes, hereafter bins, will have a cumulative form  $F$  such that  $n \leq \Sigma F \leq nk$  or, when normalised,  $1 \leq \Sigma F/n \leq k$ . When  $\Sigma F/n = 1$ , then  $f$  and  $F$  must be maximally shifted to the right, i.e., having values of 0 for all bins except the right-most. For example, letting  $k = 3$ :

$$\begin{aligned} &\text{if } f = [0, 0, n], \\ &\text{then } F = [0, 0, n], \\ &\text{and } \Sigma F/n = n/n = 1 \end{aligned}$$

Conversely, when  $\Sigma F/n = k$ , then  $F$  must have values of  $n$  for all bins and  $f$  must be maximally shifted to the left, i.e., having values of 0 for all bins except the left-most:

$$\begin{aligned} \text{If } f &= [n, 0, 0], \\ \text{then } F &= [n, n, n], \\ \text{and } \Sigma F/n &= (3 \cdot n) / n = 3 = k \end{aligned}$$

Subtracting 1 from  $\Sigma F/n$ , the resulting value represents the shift of  $f$  away from the right-most bin or, alternatively, towards the left-most bin:

$$\begin{aligned} \text{If } f &= [0, 0, n], \text{ then } \Sigma F/n = 1 - 1 = 0 \\ \text{If } f &= [n, 0, 0], \text{ then } \Sigma F/n = k - 1 = 2 \end{aligned}$$

Values of  $\Sigma F/n - 1$  can then be divided by  $k - 1$  to produce normalised values of distributional shift (DS) that range between 0 and 1, inclusive:

$$\text{DS} = (\Sigma F/n - 1) / (k - 1) \tag{1}$$

For example, given  $n = 3$  observations distributed among  $k = 3$  bins, let  $f_1 = [1, 1, 1]$  and  $f_2 = [2, 1, 0]$ . The cumulative forms of  $f_1$  and  $f_2$  are  $F_1 = [1, 2, 3]$  and  $F_2 = [2, 3, 3]$ , respectively.

Calculating DS for  $F_1$  and  $F_2$ :

$$\begin{aligned} \text{DS}(F_1) &= (\Sigma F_1/n - 1) / (k - 1) \\ &= (6/3 - 1) / (3 - 1) \\ &= 0.5 \\ \text{DS}(F_2) &= (\Sigma F_2/n - 1) / (k - 1) \\ &= (8/3 - 1) / (3 - 1) \\ &= 0.8\bar{3} \end{aligned}$$

Hence,  $f_2$  is shifted further left than  $f_1$ . More precisely,  $f_1$  is shifted to 50% of the possible maximum while  $f_2$  is shifted to ~83.3% of the possible maximum. However, as formulated in

equation 1, values of DS will not necessarily differ among non-identical distributions satisfying the same values of  $n$  and  $k$ . For example, consider the feasible set of all possible discrete cumulative frequency distributions for  $n = 3$  and  $k = 3$ , i.e.,  $A_{n=3,k=3}$ . Listed in lexicographical order, the 10 members of this feasible set and their values of DS are:

$$\begin{aligned}
F_1 &= [0, 0, 3], & \text{DS} &= 0.0 \\
F_2 &= [0, 1, 3], & \text{DS} &= 0.1\bar{6}\bar{6} \\
F_3 &= [0, 2, 3], & \text{DS} &= 0.\bar{3}\bar{3} \\
F_4 &= [0, 3, 3], & \text{DS} &= 0.5 \\
F_5 &= [1, 1, 3], & \text{DS} &= 0.\bar{3}\bar{3} \\
F_6 &= [1, 2, 3], & \text{DS} &= 0.5 \\
F_7 &= [1, 3, 3], & \text{DS} &= 0.\bar{6}\bar{6} \\
F_8 &= [2, 2, 3], & \text{DS} &= 0.\bar{6}\bar{6} \\
F_9 &= [2, 3, 3], & \text{DS} &= 0.8\bar{3}\bar{3} \\
F_{10} &= [3, 3, 3], & \text{DS} &= 1.0
\end{aligned}$$

While all 10 members of  $A_{n=3,k=3}$  are unique, there are only 7 unique values of DS. Consequently, two non-identical distributions could be interpreted as equally shifted towards the left-most bin. While this property does not necessarily invalidate a measure (e.g., two non-identical distributions can have the same mean, variance, etc.), unique values of DS can be obtained by exponentiating the cumulative frequencies to a power greater than 1, that is,  $\Sigma F^z$ , where  $z > 1$ . Normalised values can then be obtained using  $\Sigma F^z/n^z$ . Letting  $z = 2$ , consider the feasible set of discrete cumulative distributions for  $n = 3$  and  $k = 3$ :

$$\begin{aligned}
F_1 &= [0, 0, 3], & \Sigma F_1/n &= 1.00, & \Sigma(F_1^2)/n^2 &= 1.00 \\
F_2 &= [0, 1, 3], & \Sigma F_2/n &= 1.\bar{3}\bar{3}, & \Sigma(F_2^2)/n^2 &= 1.11 \\
F_3 &= [0, 2, 3], & \Sigma F_3/n &= 1.\bar{6}\bar{6}, & \Sigma(F_3^2)/n^2 &= 1.44 \\
F_4 &= [0, 3, 3], & \Sigma F_4/n &= 2.00, & \Sigma(F_4^2)/n^2 &= 2.00 \\
F_5 &= [1, 1, 3], & \Sigma F_5/n &= 1.\bar{6}\bar{6}, & \Sigma(F_5^2)/n^2 &= 1.22 \\
F_6 &= [1, 2, 3], & \Sigma F_6/n &= 2.00, & \Sigma(F_6^2)/n^2 &= 1.55 \\
F_7 &= [1, 3, 3], & \Sigma F_7/n &= 2.\bar{3}\bar{3}, & \Sigma(F_7^2)/n^2 &= 2.11 \\
F_8 &= [2, 2, 3], & \Sigma F_8/n &= 2.\bar{3}\bar{3}, & \Sigma(F_8^2)/n^2 &= 1.88 \\
F_9 &= [2, 3, 3], & \Sigma F_9/n &= 2.\bar{6}\bar{6}, & \Sigma(F_9^2)/n^2 &= 2.44 \\
F_{10} &= [3, 3, 3], & \Sigma F_{10}/n &= 3.00, & \Sigma(F_{10}^2)/n^2 &= 3.00
\end{aligned}$$

Here, each value of  $\Sigma F^z/n^z$ , is unique and the original lower and upper constraints on  $\Sigma F/n$  are retained. Reformulating DS:

$$DS = (\Sigma F^z/n^z - 1) / (k - 1) \quad (2)$$

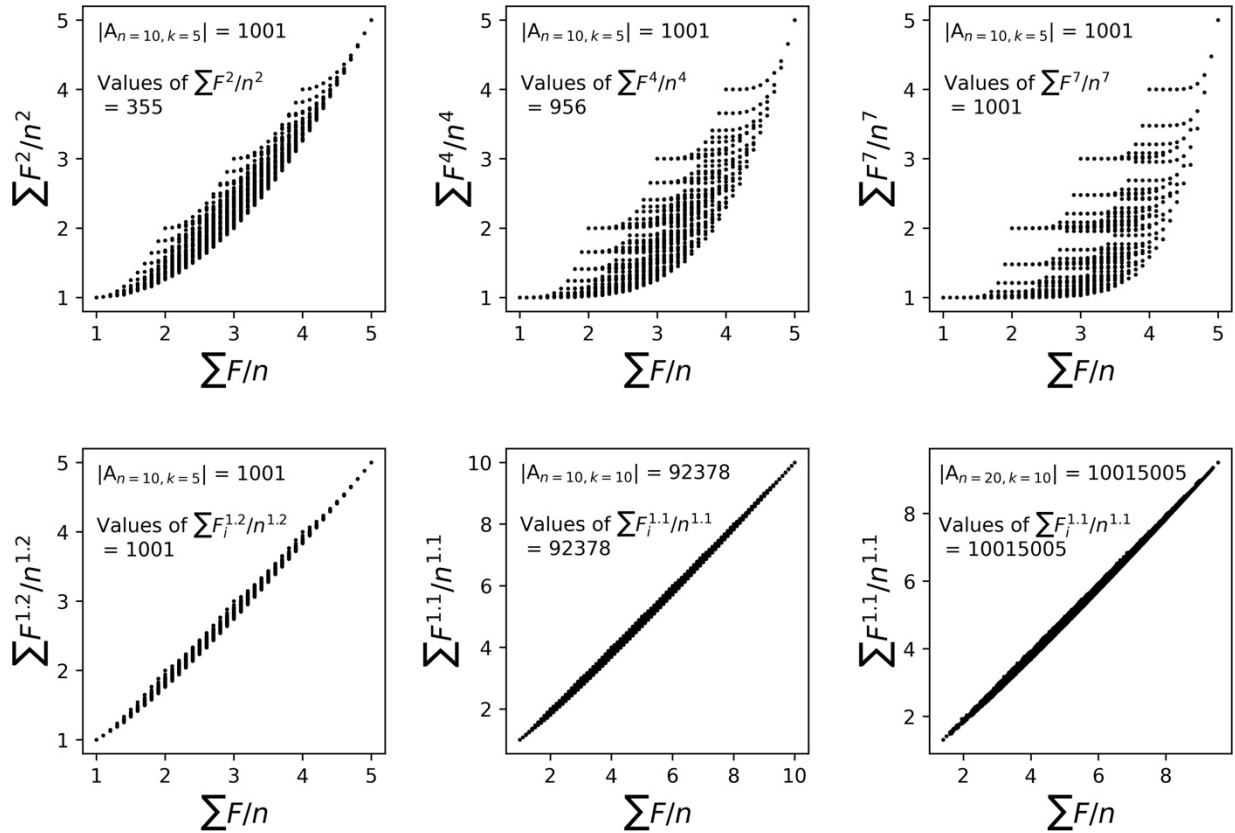
Arbitrarily chosen exponents do not, however, ensure the uniqueness of  $\Sigma F^z/n^z$  among distributions having identical  $n$  and  $k$ , and may produce unreasonable outcomes. For example, consider the subset of the feasible set for  $n = 5$  and  $k = 4$ , where  $\Sigma F/n = 2.2$ :

$$\begin{aligned} F_1 &= [0, 1, 5, 5], & \Sigma F_1/n &= 2.2, & \Sigma(F_1^2)/n^2 &= 2.04, & \Sigma(F_1^3)/n^3 &= 2.008 \\ F_2 &= [0, 2, 4, 5], & \Sigma F_2/n &= 2.2, & \Sigma(F_2^2)/n^2 &= 1.8, & \Sigma(F_2^3)/n^3 &= 1.576 \\ F_3 &= [0, 3, 3, 5], & \Sigma F_3/n &= 2.2, & \Sigma(F_3^2)/n^2 &= 1.72, & \Sigma(F_3^3)/n^3 &= 1.432 \\ F_4 &= [1, 1, 4, 5], & \Sigma F_4/n &= 2.2, & \Sigma(F_4^2)/n^2 &= 1.72, & \Sigma(F_4^3)/n^3 &= 1.528 \\ F_5 &= [1, 2, 3, 5], & \Sigma F_5/n &= 2.2, & \Sigma(F_5^2)/n^2 &= 1.56, & \Sigma(F_5^3)/n^3 &= 1.288 \\ F_6 &= [2, 2, 2, 5], & \Sigma F_6/n &= 2.2, & \Sigma(F_6^2)/n^2 &= 1.48, & \Sigma(F_6^3)/n^3 &= 1.192 \end{aligned}$$

Using  $z = 2$  produces  $\Sigma F^z/n^z = 1.72$  for both  $F_3$  and  $F_4$ . However, unique values of  $\Sigma F^z/n^z$  are obtained when using  $z = 3$ , whereby recalculating DS for  $F_3$  and  $F_4$  produces  $DS(F_3) = 0.144$  and  $DS(F_4) = 0.176$ . This result indicates that  $F_4$  is shifted left of  $F_3$ , which may not be intuitive since a greater fraction of  $n$  is shifted left of centre in  $F_3$ . Consequently, while larger exponents may produce unique values of  $\Sigma F^z/n^z$ , they can also inflate minor differences between distributions (Fig 1). Fortunately, this undesirable effect can be avoided with a fractional exponent. Specifically, using  $z = (k + 1)/k$  makes  $z$  dependent on  $k$  while avoiding large exponents (Fig 1). Reformulating DS:

$$DS = (\Sigma F^{(k+1)/k} / n^{(k+1)/k} - 1) / (k - 1) \quad (3)$$

**Figure 1.** Top: Normalised sums of exponentiated cumulative frequencies ( $\Sigma F^z/n^z$ ) for distributions having 10 observations distributed among 5 bins (i.e.,  $A_{n=10,k=5}$ ), the feasible set for which contains 1001 unique distributions. Bottom: Values of  $\Sigma F^z/n^z$ , where  $z = (k+1)/k$ . In each case, the number of unique values of  $\Sigma F^z/n^z$  equals the cardinality of the feasible set,  $|A|$ .



Though using  $z = (k + 1)/k$  produces unique values of DS for all combinations of  $n \leq 200$  and  $k \leq 20$  where  $|A_{n,k}| < 2 \cdot 10^7$ , we cannot mathematically prove that such will be the case for all combinations of arbitrarily large  $n$  and  $k$ . If such is not the case and if uniqueness is strictly necessary, then the exponent of DS will need to be revised.

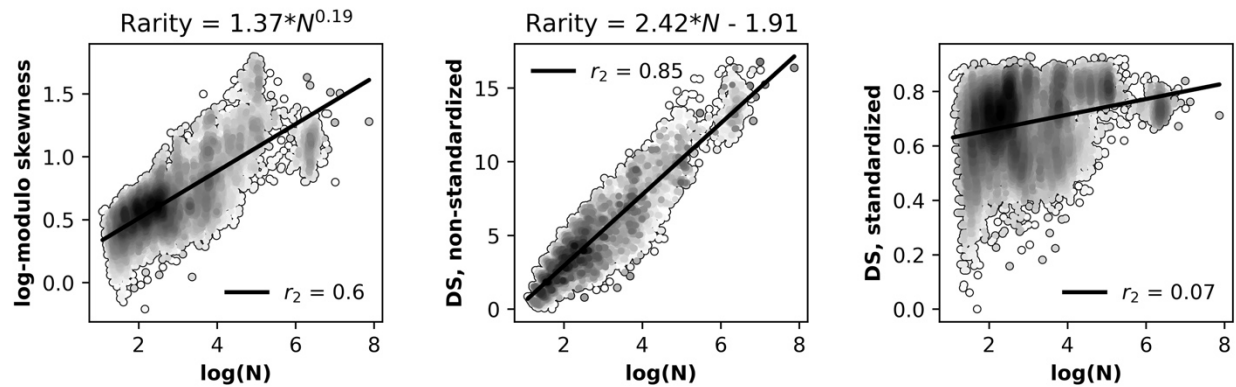
## 2.2 DS as a measure of species rarity

A species abundance distribution (SAD) is a histogram of abundances sampled from an ecological community, e.g., trees of a forest, mammals of a desert. SADs underpin thousands of ecological studies, are central to theories of biodiversity, and are the basis for many biodiversity measures (Magurran and McGill, 2010; McGill et al., 2010, Locey and White 2013).

Here, we demonstrate the use of DS as a measure of species rarity ( $R$ ) using data from a study of 44,090 communities of plants, animals, fungi, and bacteria (i.e., Lennon and Locey, 2020). That study used a compilation of data from two prior studies (i.e., Locey and Lennon, 2016; Louca et al., 2019). Studies by Locey and Lennon (2016, 2020) measured  $R$  via a log-modulo transformation of skewness and supported a statistical scaling of  $R$  with total sample abundance ( $N$ ):  $R \propto N^z$ . See Appendix 1 of the Supplemental file for details on datasets and methodology.

Reanalyzing data of Lennon and Locey (2020), the non-standardised form of DS (i.e.,  $\sum F^{(k+1)/k} / n^{(k+1)/k} - 1$ ) explained nearly 85% of variation in  $\log(N)$  compared to nearly 60% explained via the log-modulo skewness measure (Fig 2). The standardised form of DS, i.e.,  $(\sum F^{(k+1)/k} / n^{(k+1)/k} - 1) / (k - 1)$ , was however poorly related to  $N$  (Fig 2). This latter result emerged because the abundance of the most abundant species strongly scales with  $N$  (see Locey and Lennon 2016). Hence, an arbitrarily large increase in  $N$  will often increase the number of bins ( $k$ ) in the SAD. By dividing the non-standardised measure of DS (i.e.,  $\sum F^{(k+1)/k} / n^{(k+1)/k} - 1$ ) by  $k - 1$ , the standardised measure lessens the indirect influence of  $N$  on  $R$ . While the standardised measure of DS produced a weaker relationship to  $N$ , it may be the preferred measure of rarity when the effect of  $N$  is to be controlled for.

**Figure 2.** Relationships of species rarity to total sample abundance ( $N$ ). Left: A previously documented rarity-abundance scaling relationship (Locey and Lennon 2016, Lennon and Locey 2020). Centre: Rarity measured via the non-standardised version of distributional shift (DS). Right: Rarity measured via the standardised version of DS.



### 2.3 DS as a measure of poverty

Numerous measures are used to examine distributions of wealth on the basis of inequality and poverty (Table 2) (Haughton and Khandker, 2009; Foster et al., 2010). However, while measures of inequality (e.g., Gini index) are solely based on statistical dispersion (Williams and Doessel, 2006), poverty measures are invariably based on poverty lines (Table 2) (Haughton and Khandker, 2009; Foster et al., 2010). For example, US poverty lines are based on estimated costs of adequate food intake for families of specific sizes; these annually updated estimates are multiplied by 3 to derive the poverty line (Haughton and Khandker 2009). Though oversimplified, US poverty lines determine whether families qualify for forms of federal assistance (United States Department of Health and Human Services, 2024).

**Table 2.** Poverty measures. Each relies on a poverty line. The poverty rate, poverty gap index, and poverty severity index belong to the family of Foster–Greer–Thorbecke indices. Equations for each measure are based on Haughton and Khandker (2009).

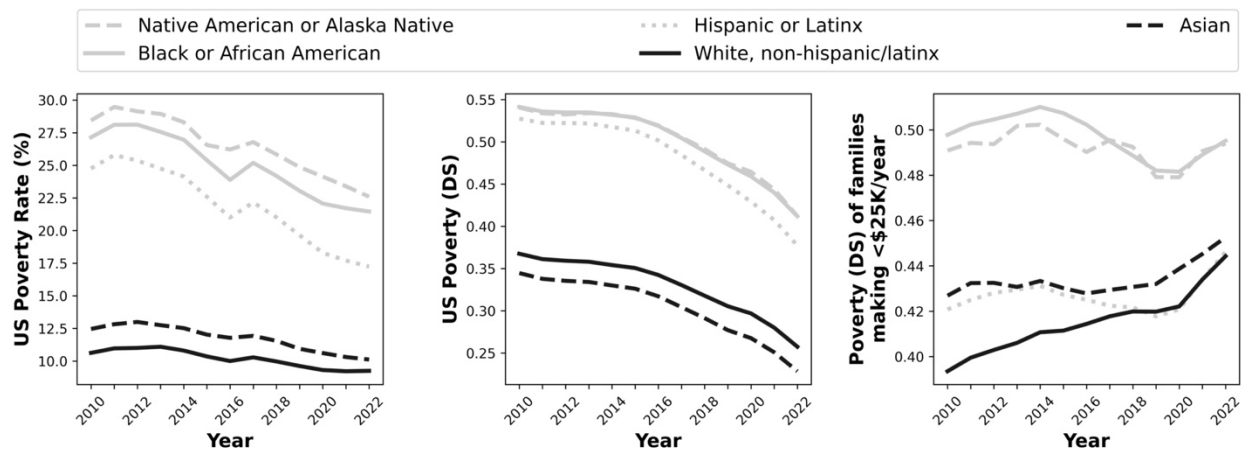
Measure	Equation	Description
Poverty rate, i.e., head count ratio	$P_0 = \frac{N_P}{N}$	The number of impoverished people, families, etc. ( $N_P$ ) divided by the number of people, families, etc. ( $N$ ).
Poverty Gap Index	$P_1 = \frac{1}{N} \sum_{i=1}^N \frac{G_i}{z}$	Normalised sum of ratios between individual poverty gaps ( $G_i$ ) and the poverty line ( $z$ ), where $G_i = z - y_i$ and $y_i$ is the income of the $i^{\text{th}}$ individual, family, etc.
Poverty Severity Index	$P_2 = \frac{1}{N} \sum_{i=1}^N \left( \frac{G_i}{z} \right)^2$	Similar to the $P_1$ but based on a normalised sum of squares.
Sen Index	$P_S = P_0 \left( 1 - (1 - G^P) \frac{\mu^P}{z} \right)$	A combination of poverty rate ( $P_0$ ) and Gini's inequality index ( $G$ ), where $G^P$ is inequality among the poor and $\mu^P$ is the mean income among the poor.
Sen-Shorrocks-Thon Index	$P_{SST} = P_0 P_1^P (1 + \hat{G}^P)$	The product of poverty rate, the poverty gap index (only including the poor), and 1 plus the Gini coefficient of the poverty gap ratios for the entire population.
Watts Index	$W = \frac{1}{N} \sum_{i=1}^P \ln \left( \frac{z}{y_i} \right)$	Normalised sum of logarithmically transformed ratios of the poverty line ( $z$ ) to individual income ( $y_i$ ) for all individuals qualifying as poor ( $P$ ).

Similarly over-simplified is the means by which US poverty is commonly reported, i.e., the poverty rate (Table 2). Although intuitive, poverty rates do not reveal how poor the poor are when compared to the rest of the population, i.e., relative poverty (Haughton and Khandker, 2009). Unlike inequality measures, poverty rates and other measures of poverty cannot be easily calculated for distributions of wealth based on assets, commodities, natural resources, human capital, or family incomes for different nations. Consequently, we examined DS as a statistically global and generalisable measure of poverty.

For this analysis, we used data on family incomes and poverty rates from the United States Census Bureau American Community Survey (United States Census Bureau, 2024a,b). These data included 13 census years (2010 to 2022) and 16 bins of 2020 inflation-corrected family incomes (see Appendix 2 of the Supplement for greater details). From these data, we used five categories of single race/ethnicity households: Hispanic or Latinx, White not Hispanic or Latinx, Asian, Black or African American, Native American or Alaskan Native.

Longitudinal patterns of DS reflected the general decrease in official US poverty rates (Fig 3). Since 2010, Native American, Alaska Native, and Black or African American families have experienced greater poverty than Asian and White non-Hispanic/Latinx families (Fig 3). White non-Hispanic/Latinx families had the lowest poverty rates but Asian families had the lowest shift towards poverty, revealing the effect of relative poverty (i.e., distribution of wealth among families that are not technically poor) (Fig 3). While official US poverty rates have generally decreased since 2010, use of DS revealed that the poorest families have gotten poorer, especially since the onset of COVID-19 (Fig 3).

**Figure 3.** Left: Official US poverty rates. Centre: Poverty measured as distributional shift (DS). Right: Poverty (DS) for families with annual incomes less than \$25K.



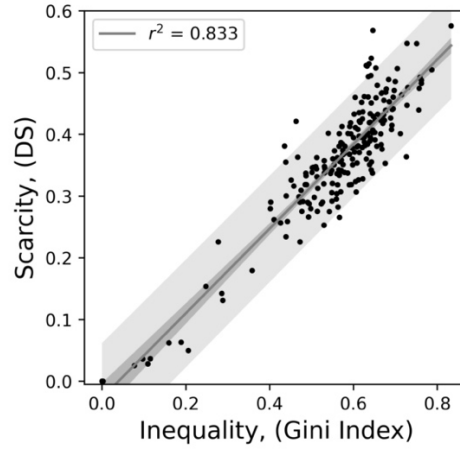
## **2.4 DS as a measure of scarcity**

Measures of scarcity are generally based on ratios (e.g., population sex ratios, ratio of water demand to availability) or composites of ratios and other measures (Ember and Ember, 1992; Rijsberman, 2006; Edalat and Stephen, 2019; Jackson et al., 2020). Unlike measures of inequality, measures of scarcity are rarely, if ever, based on general statistical properties of frequency distributions. However, such a measure may provide a generalisable complement to measures of inequality and provide information on distributions of wealth and resources that other measures of scarcity do not.

We examined DS as a measure of scarcity using data on the production of 209 food commodities (e.g., wheat, rice, chicken meat) among 200 nations in 2022. We obtained these publicly available data from the United Nations Food and Agriculture Organization website (United Nations, Food and Agriculture Organization, 2024). We then calculated DS and the Gini coefficient of inequality with respect to each of the 209 food commodities. See Appendix 3 of the Supplemental file for greater details on data and methodology.

We found that greater inequality in food production was positively associated with greater scarcity in food production and hence, a greater fraction of nations that produced relatively little ( $r^2 = 0.833$ ,  $p < 0.001$ ) (Fig 4). However, scarcity (i.e., DS) sometimes took a considerable range of values for a given value of inequality (i.e., the Gini coefficient). For example, at an inequality of nearly 0.62, scarcity ranged from nearly 0.3 to nearly 0.56 (Fig 4). As two distributions (e.g., representing two commodities or the same commodity examined in two different years) may have similar inequality but greatly differ in scarcity, both properties may be important to measure.

**Figure 4.** Scarcity of food production measured as distributional shift (DS), versus inequality in food production. Each dots represents one of 209 food commodities.



### 3. Relative distributional shift (RDS)

#### 3.1 RDS as a simple difference in DS

Given two discrete cumulative distributions,  $F_1$  and  $F_2$ , satisfying the same  $n$  and  $k$ , the shift of  $F_1$  relative to  $F_2$  can be measured as a simple difference, that is, as relative distributional shift (RDS), where  $RDS = DS(F_2) - DS(F_1)$ . As the minimum possible value for DS is 0 and the maximum is 1, RDS is constrained to a minimum and maximum signed difference, i.e.,  $-1 \leq RDS \leq 1$ . The sign and magnitude of RDS represents the degree to which  $F_1$  is shifted right or left of  $F_2$ . For example, given  $n = 10$ ,  $k = 3$ , and letting  $f_1 = [10, 0, 0]$  and  $f_2 = [0, 0, 10]$ :

$$\begin{aligned} DS(F_1) &= (\sum F_1^{(k+1)/k} / n^{(k+1)/k} - 1) / (k - 1) \\ &= [(3 \cdot 10^{(3+1)/3}) / 10^{(3+1)/3} - 1] / (3 - 1) \\ &= (3 - 1) / (3 - 1) = 1 \end{aligned}$$

$$\begin{aligned} DS(F_2) &= (\sum F_2^{(k+1)/k} / n^{(k+1)/k} - 1) / (k - 1) \\ &= (10^{(3+1)/3} / 10^{(3+1)/3} - 1) / (3 - 1) \\ &= (1 - 1) / (3 - 1) = 0 \end{aligned}$$

Therefore,  $RDS = DS(F_2) - DS(F_1) = -1$ . The sign of RDS indicates that  $F_1$  is shifted left of  $F_2$ , while the absolute value of RDS takes the maximum possible absolute difference of 1. Taken together,  $F_1$  cannot be shifted more to the left of  $F_2$ . Importantly, RDS is symmetrical with respect to its absolute value, i.e.,  $|DS(F_2) - DS(F_1)| = |DS(F_1) - DS(F_2)|$ ; a generally desirable property of comparative measures (Deza and Deza 2014).

### ***3.2 Relationships of RDS to comparative measures***

We asked how RDS relates to popular measures of distance, divergence, intersection, and probabilistic scoring. These measures are widely used in fields such as ecology (Legendre and Legendre, 2012; Simonis et al., 2021), medicine and medical imaging (Tan et al., 2013; Pasnoori et al., 2024), bioinformatics (Luczak et al., 2019; Ramsden, 2023), and the general practice of image analysis and machine learning (Murphy, 2012; Szeliski, 2022). However, while RDS is based on the difference in a global property (i.e., DS) and can take negative values, established measures are calculated via pairwise differences between corresponding bins or discrete classes, and are restricted to non-negative values.

We examined relationships of RDS to Chi-square distance (CSD), Kullback-Leibler divergence (KLD), Kolmogorov-Smirnov distance (KSD), earth mover's distance (EMD), ranked probability score (RPS), and histogram *non*-intersection ( $1 - HI$ ) (Table 1) (Murphy, 1970; Deza and Deza, 2014; Asha et al., 2011). We explored the effects of binning (i.e.,  $k$ ) and the shape of the population distribution on the relationship of RDS to other measures using the one-parameter Weibull distribution of the NumPy numerical computing library. This distribution was ideal, as the single parameter ( $\alpha$ ) can produce a variety of shapes, e.g.,  $\alpha = 0.5$  produces a rapidly decreasing monotonic function;  $\alpha = 1$  produces an exponential distribution;  $\alpha = 3.5$

produces a symmetrical unimodal distribution;  $\alpha = 20$  produces a highly left-skewed distribution with an internal mode. As the one-parameter Weibull distribution is continuous, it is also more amenable to exploring the effects of binning than a discrete distribution.

For each combination of  $\alpha = (0.5, 1, 3.5, 20)$  and  $k = (5, 10, 20, 40)$ , we conducted  $10^5$  comparisons on pairs of independent random samples ( $n = 100$ ). We used a small value for  $n$  to ensure high sampling error and hence, high variation among samples. We calculated RDS, EMD, RPS, KSD, KLD, CSD, and  $1 - \text{HI}$  for each pair of random samples. We then performed ordinary least squares regressions using absolute RDS, i.e.,  $|\text{RDS}|$ . For CSD, KLD, and RPS, regressions were based on the square roots of those measures, as distributions of their values were highly skewed (i.e., few extremely high values and many low values) relative to other measures. Additionally, as CSD and KLD cannot be computed when the values of corresponding bins are zero, we applied add-one smoothing when calculating CSD and KLD.

We found that  $|\text{RDS}|$  was most strongly related to EMD, ( $0.93 \leq r^2 \leq 0.97, p < 0.001$ ) and RPS ( $0.92 \leq r^2 \leq 0.96, p < 0.001$ ); neither  $\alpha$  nor  $k$  had a substantial effect on the relationship between  $|\text{RDS}|$  and these measures (Fig 5, Fig 6). However,  $|\text{RDS}|$  was less related to KSD ( $0.66 \leq r^2 \leq 0.89, p < 0.001$ ) and the relationship was weakened by the combined effect of decreased  $\alpha$  (i.e., greater right-skew) and increased  $k$  (i.e., greater numbers of bins) (Fig 5, Fig 6).

Relationships of  $|\text{RDS}|$  to the square roots of KLD and CSD were highly variable ( $0.25 \leq r^2 \leq 0.82, p < 0.001$ ) and were also weakened by decreased  $\alpha$  and increased  $k$  (Fig 5, Fig 6). The relationship of  $|\text{RSD}|$  to  $1 - \text{HI}$  was also highly variable ( $0.24 \leq r^2 \leq 0.77, p < 0.001$ ) and weakened by increased  $k$ , but was strongest for values of  $\alpha$  corresponding to the most skewed distributions, i.e.,  $\alpha = (0.5, 20)$  (Fig 5, Fig 6).

**Figure 5.** Coefficients of determination ( $r^2$ ) from relationships of absolute relative distributional shift, |RDS|, to earth mover's distance (EMD), ranked probability score (RPS), Kolmogorov-Smirnov distance (KSD), Kullback-Leibler divergence (KLD), histogram non-intersection (1 - HI), and Chi-square distance (CSD).

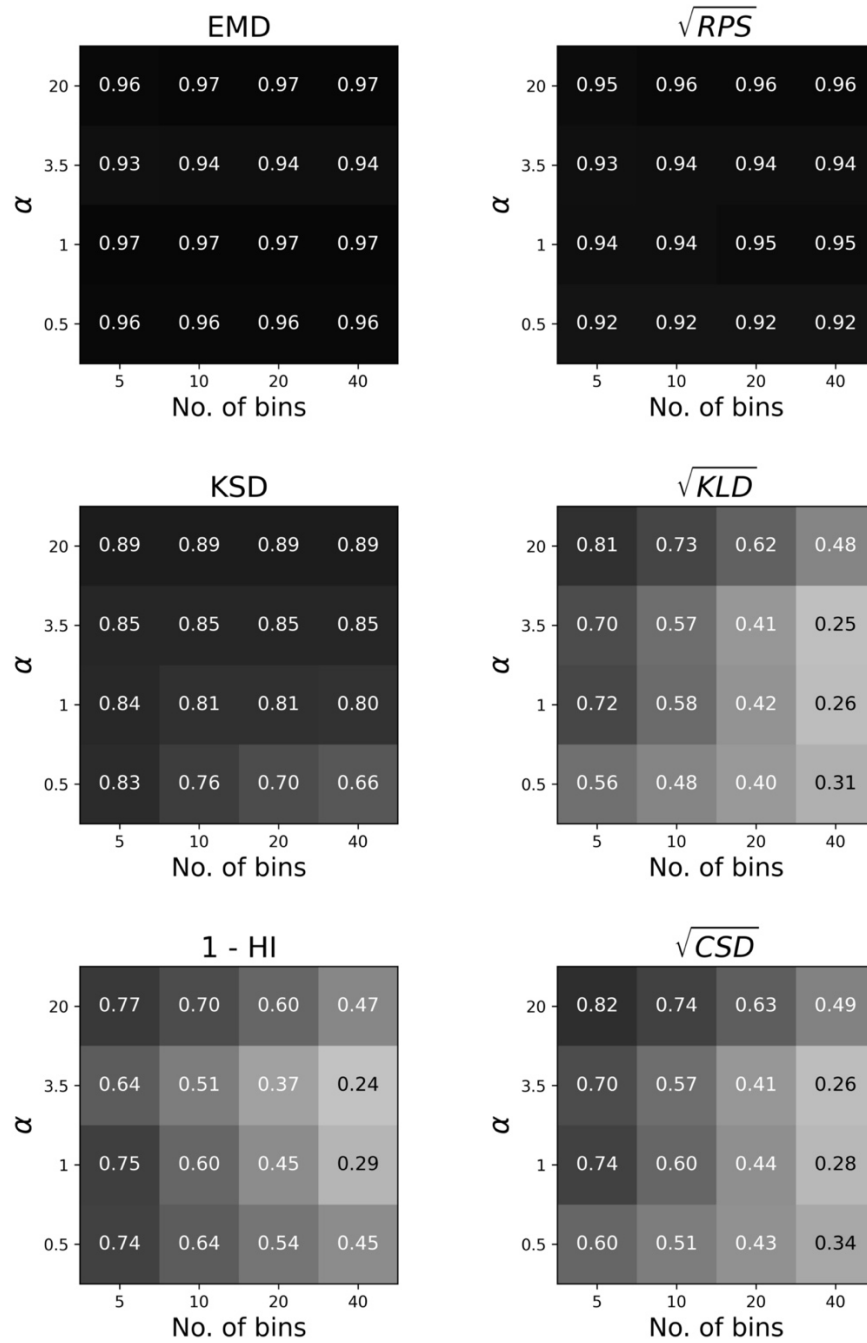
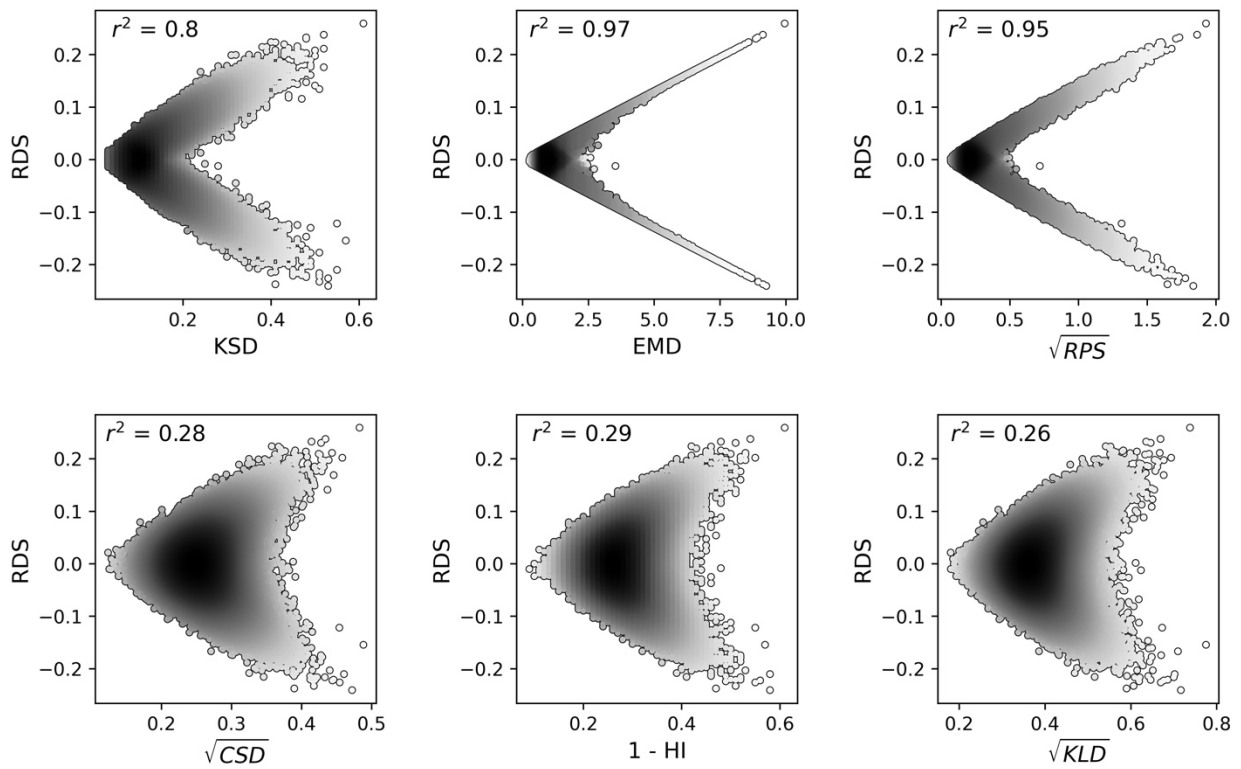


**Figure 6.** Relationships of relative distributional shift (RDS) to Kolmogorov-Smirnov distance (KSD), earth mover’s distance (EMD), ranked probability score (RPS), Chi-square distance (CSD), histogram non-intersection ( $1 - HI$ ), and Kullback-Leibler divergence (KLD). Each data point represents a comparison of two histograms, each generated via random samples of the one-parameter Weibull distribution ( $\alpha = 1, k = 40, n = 100$ ). Coefficients of determination ( $r^2$ ) are based on ordinary least squares regression performed using  $|RDS|$ .



RDS often remained near zero when values of CSD,  $1 - HI$ , and KLD were relatively high (Fig 6). This latter result revealed an important nuance of measuring DS. Specifically, differences in shape do not imply differences in shift. For example, letting  $n = 46$  and  $k = 5$ , consider the case when  $f_1 = [21, 2, 0, 2, 21]$  and  $f_2 = [1, 1, 42, 1, 1]$ . For  $f_1$ , nearly 45.7% of  $n$  is shifted entirely left while nearly 45.7% remains in the right-most bin. For  $f_2$ , nearly 91.3% of  $n$  is

shifted 50% left, essentially splitting the difference present in  $f_1$ . Because of this, DS for  $f_1$  and  $f_2$  are somewhat similar,  $DS(f_1) = 0.435$ ,  $DS(f_2) = 0.489$ , resulting in a low value for RDS (0.053) despite the disparate shapes of  $f_1$  and  $f_2$ . Calculating  $1 - HI$  for  $f_1$  and  $f_2$  produces 91.3% non-overlap. Consequently,  $f_1$  and  $f_2$  have disparate shapes but similar shift.

### ***3.3 Application of RDS to image analysis***

Measures of distance, divergence, intersection, and probabilistic scoring are commonly used to compare images based on, e.g., histograms of pixel values representing colours (Cassisi et al., 2012; Murphy, 2012; Liu and Yang, 2021; Szeliski, 2022). RDS may be highly relevant to image analysis due to its indication of directional shifts, e.g., in the colour spectrum. As an exploratory demonstration, we compared RDS to EMD,  $1 - HI$ , CSD, KLD, KSD, and RPS in regard to detection of events, signals, and patterns within 34 mp4-formatted video files obtained from Pexels (<https://www.pexels.com/>) and Pixabay (<https://pixabay.com/>). Each service offers free stock videos licensed for non-commercial use.

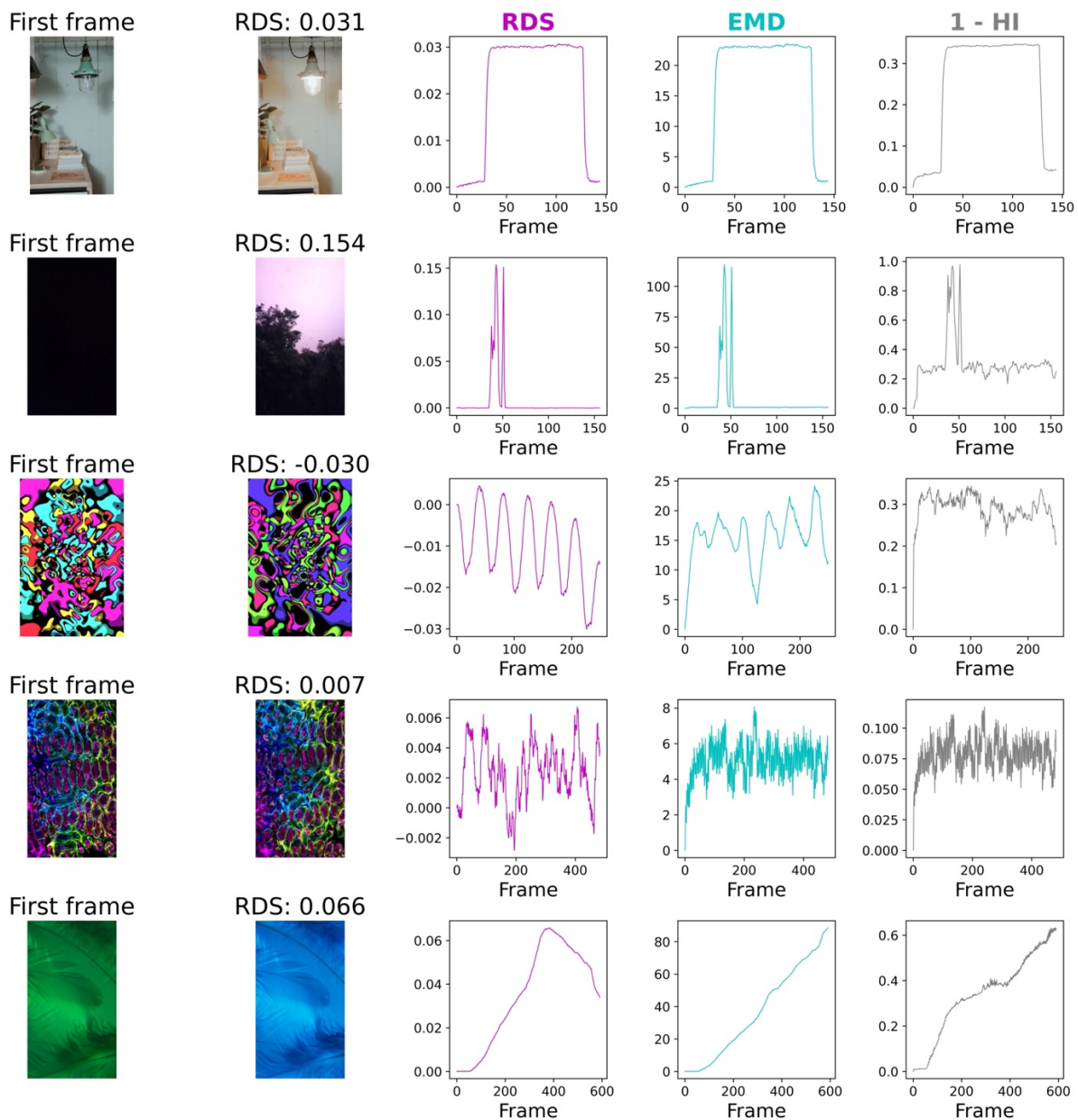
We used the OpenCV (v4.9.0.80) computer vision library to decompose each video into individual image frames, and to construct three 256-bin colour histograms for the three bands of RGB colour values (Bradski, 2000). One dimensional colour histograms were then formed by concatenating histograms for the three bands in R, G, B order (Cassisi et al., 2012). For each video, we used the first frame as a reference against which subsequent frames were compared. See Appendix 4 of the Supplemental file for additional details. Results for three measures (i.e., RDS, EMD,  $1 - HI$ ) and five videos are presented in Figure 7; results for all videos and all measures are presented in Supplemental figures 1-34.

First, to compare the detection of a simple light event, we used a six second video wherein a light bulb is turned on and then off after four seconds. Here, each measure registered little change until the bulb was turned on, which resulted in a rapid change that quickly plateaued until the light was turned off (Fig 7, Supplemental Figure 1). Second, to compare the detection of erratic bursts of light, we used a six-second video featuring a burst of lightening strikes. Here, RDS, EMD, and RPS registered little change on either side of the burst, while 1 – HI, CSD, KSD, and KLD registered considerable noise (Fig 7, Supplemental Figure 2).

Third, to compare detection of changes in complex colour patterns, we used a 10 second video wherein amorphously changing shapes visually shifted from hues of red, to orange, yellow, green, blue, purple, magenta, and back to red in synchronous and asynchronous fashion. Here, RDS detected a clear sinusoidal signal while EMD and RPS detected two sets of irregular spikes (Fig 7, Supplemental Figure 3). CSD, KSD, and KLD detected two sets of irregular spikes but also substantial noise, while 1 – HI detected no apparent pattern (Fig 7, Supplemental Figure 3). Fourth, we used a digital art video resembling an animation of fluorescent cell imaging to examine whether each measure could detect a signal in seemingly stochastic high-contrast colour changes. While no measure detected a patterned signal, RDS detected a clearer signal than all other measures (Fig 7, Supplemental Figure 4).

Fifth, for a demonstration of detection of red-shift and blue-shift, we used a video wherein a static image transitioned through shades of colour. Here, RDS was the only measure that registered an internal mode, i.e., a gradual blue-shift away from the reference image followed by a gradual red-shift towards the reference image (Fig 7, Supplemental Figure 5). All other measures registered a nearly monotonic increase in difference from the reference image (Fig 7, Supplemental Figure 5).

**Figure 7.** Detection of events and colour changes in videos. Row 1: A light bulb turns on, then off. Row 2: Short burst of lightening strikes. Row 3: Patterned changes in amorphous shapes. Row 4: Colours changes among images resembling fluorescent cell imaging. Row 5: Whole image colours shifts. For each row, the first column is the first video frame and the reference image against which other frames are compared. The second column is the frame with the greatest  $|RDS|$  value. The remaining columns correspond to RDS, EMD, and  $1 - HI$ .



In general, RDS performed as well as or better than other measures in detecting signals and patterns (Fig 7, Supplemental Figures 1 – 34). Because RDS is signed, it is uniquely able to distinguish red-shifts from blue-shifts (Fig 7, Supplemental figures 5 – 11). RDS was often better able to detect signals among complex images (Fig 7, Supplemental figures 3, 4, 12, 13). When other measures detected abrupt changes, RDS often detected smoother signals of directional shift (Supplemental figures 14 – 22). RDS also performed as well as or better than other measures in detecting animal activity (Supplemental figures 23 – 27). When examining videos of visual noise, RDS varied from detecting signals and patterns that were similar to those of other measures, to detecting patterns when other measures detected noise and *vice versa* (Supplemental figures 28 – 34).

#### **4. Discussion**

The concept of shift is commonly invoked when comparing statistical moments, frequency distributions, and histograms but had not yet been established as a property of individual distributions. We defined distributional shift (DS) as the concentration of frequencies towards the lowest discrete class (e.g., the left-most bin of a histogram), which we quantified as a normalised sum of exponentiated cumulative frequencies. Realising the link between DS and concepts of rarity, poverty, and scarcity, we demonstrated advantages of using DS to measure these properties. We then defined relative distributional shift (RDS) to reveal the magnitude and direction by which one distribution is shifted relative to another; a unique property among comparative measures.

Despite being a signed measure, RDS is symmetrical with respect to its absolute value, i.e.,  $|\text{RDS}|$ , meaning that the order in which distributions are compared does not affect  $|\text{RDS}|$ .

This desirable property is also satisfied by measures such as earth mover's distance, ranked probability score, Kolmogorov-Smirnov distance, Chi-square distance, and histogram non-intersection. By contrast, Kullback-Leibler divergence is an asymmetrical measure. The consistently strong statistical relationships of RDS to earth mover's distance and ranked probability score suggests that RDS may be a useful alternative to these measures when directional differences are of interest.

The ability of RDS to quantify both the direction and magnitude of difference makes it particularly useful for image analysis in detecting, e.g., red-shifts, blue-shifts, and patterns within signals. In videos involving complex colour changes, RDS was able to detect patterns or produce clear signals when other measures did not. While RDS may prove to be useful in other areas of image analysis where comparative measures of histograms are commonly used (e.g., image classification), the ability of RDS to detect events, patterns, and to signal temporal shifts may lend it to applications of longitudinal comparisons outside of image analysis, e.g., in ecological forecasting and the broader field of time-series analysis.

Despite presenting multiple lines of evidence for the usefulness of DS in characterizing individual distributions and of RDS in distributional comparisons, our study had limitations. First, we derived and applied DS and RDS in relation to discrete frequency distributions and histograms. We did not explore the generalisation of DS and RDS to continuous distributions. Second, our analyses were largely exploratory demonstrations, and not in-depth studies of individual applications. In particular, formal image analyses often include complex analytical pipelines involving extensive data cleaning and optimization, as well diagnostic tests (e.g., receiver operating characteristics).

In conclusion, distributional shift as defined in the current work is a novel and intuitive property of individual distributions and its precise measurement yields a useful measure (i.e., DS) for characterising extreme but ubiquitous properties (e.g., poverty, rarity, scarcity) and a unique basis for a directional measure of distributional comparison (i.e., RDS). We envision that DS and RDS may also be derived differently (e.g., for continuous distributions) to measure and characterise the same general property.

### **Acknowledgments**

We thank Dr.'s Ethan P. White and Xiao Xiao for discussions on the comparison of RDS to other measures. We thank the individuals who collected and provided the many ecological datasets comprising the data compilations used herein, i.e., those of Locey and Lennon (2016), Louca et al. (2019), and Lennon and Locey (2020); in particular, the citizen scientists who collect Breeding Bird Survey and Christmas Bird Count data, the Earth Microbiome Project, the Human Microbiome Project, the Tara Ocean Expedition project, researchers who provided metagenomic data on MG-RAST as well as the individuals who maintain and provide the MG-RAST service, the Audubon Society, the US Forest Service, the Missouri Botanical Garden, and Alwyn H. Gentry. We also thank those who provide and maintain the freely usable Pexels and Pixabay web services and the individuals who produced the video files used in this study.

### **Availability of data and source code**

Data and source code needed to reproduce the findings and figures herein are available in a public GitHub repository: [https://github.com/Rush-Quality-Analytics/distributional\\_shift](https://github.com/Rush-Quality-Analytics/distributional_shift). This

repository does not contain original video files due to redistribution restrictions, and instead contains links to each video file and instructions for using them to reproduce our analyses.

### **Disclosure statement**

The authors declare no potential conflict of interest.

### **Supplemental File**

A pdf file containing appendices and supplemental figures is available in our institution's public GitHub repository: [https://github.com/Rush-Quality-Analytics/distributional\\_shift/blob/main/Supplement/2024\\_04\\_14\\_Supplement\\_for\\_Preprint.pdf](https://github.com/Rush-Quality-Analytics/distributional_shift/blob/main/Supplement/2024_04_14_Supplement_for_Preprint.pdf)

### **Funding**

This study was not supported by external funding.

### **References**

1. Asha, V., Bhajantri, N.U., & Nagabhushan, P. (2011). GLCM-based chi-square histogram distance for automatic detection of defects on patterned textures. *International Journal of Computer Vision and Robotics*, 2, 302-313.
2. Bradski, G. (2000). The OpenCV library. *Dr. Dobb's Journal: Software Tools for the Professional Programmer*, 25, 120-123.
3. Chen, Y., Raab, R., Wang, J., & Liu, Y. (2022). Fairness transferability subject to bounded distribution shift. *Advances in Neural Information Processing Systems*, 35, 11266-11278.

4. Colles, F.M., Cain, R.J., Nickson, T., Smith, A.L., Roberts, S.J., Maiden, M.C., Lunn, D., & Dawkins, M.S. (2016). Monitoring chicken flock behaviour provides early warning of infection by human pathogen *Campylobacter*. *Proceedings of the Royal Society B: Biological Sciences*, 283, 20152323.
5. Edalat, M.M., & Stephen, H. (2019). Socio-economic drought assessment in Lake Mead, USA, based on a multivariate standardized water-scarcity index. *Hydrological Sciences Journal*, 64, 555-569.
6. Ember, C.R., & Ember, M. (1992). Warfare, aggression, and resource problems: Cross-cultural codes. *Behavior Science Research*, 26, 169-226.
7. Deza, M.M., & Deza, E. (2014). *Encyclopedia of Distances*. Springer Berlin Heidelberg.
8. Doksum, K. (1974). Empirical probability plots and statistical inference for nonlinear models in the two-sample case. *Annals of Statistics*, 2, 267-277.
9. Duffy, S., Huttenlocher, J., Hedges, L.V., & Crawford, L.E. (2010). Category effects on stimulus estimation: Shifting and skewed frequency distributions. *Psychonomic Bulletin & Review*, 17, 224-230.
10. Foster, J., Greer, J., & Thorbecke, E. (2010). The Foster–Greer–Thorbecke (FGT) poverty measures: 25 years later. *The Journal of Economic Inequality*, 8, 491-524.
11. Haughton, J., & Khandker, S.R. (2009). *Handbook on Poverty and Inequality*. World Bank Publications, 446.
12. Gail, M.H., & Green, S.B. (1976). A generalization of the one-sided two-sample Kolmogorov-Smirnov statistic for evaluating diagnostic tests. *Biometrics*, 561-570.

13. Cassisi, C., Montalto, P., Aliotta, M., Cannata, A., & Pulvirenti, A. (2012). Similarity measures and dimensionality reduction techniques for time series data mining. In *Advances in Data Mining Knowledge Discovery and Applications*. pp. 71-96.
14. Hyam, L., Richards, K.L., Allen, K.L., & Schmidt, U. (2023). The impact of the COVID-19 pandemic on referral numbers, diagnostic mix, and symptom severity in Eating Disorder Early Intervention Services in England. *International Journal of Eating Disorders*, 56, 269-275.
15. Jackson, J.C., Gelfand, M., & Ember, C.R. (2020). A global analysis of cultural tightness in non-industrial societies. *Proceedings of the Royal Society B*, 287, 20201036.
16. Legendre, P., & Legendre, L. (2012). *Numerical Ecology*. Elsevier.
17. Lennon, J.T., & Locey, K.J. (2020). More support for Earth's massive microbiome. *Biology Direct*, 15, 1-6.
18. Liu, G.H., & Yang, J.Y. (2021). Deep-seated features histogram: A novel image retrieval method. *Pattern Recognition*, 116, 107926.
19. Locey, K.J., & Lennon, J.T. (2016). Scaling laws predict global microbial diversity. *Proceedings of the National Academy of Sciences of the United States of America*, 113, 5970-5975.
20. Locey, K.J., & White, E.P. (2013). How species richness and total abundance constrain the distribution of abundance. *Ecology Letters*, 16, 1177-1185.
21. Louca, S., Mazel, F., Doebeli, M., & Parfrey, L.W. (2019). A census-based estimate of Earth's bacterial and archaeal diversity. *PLoS Biology*, 17, e3000106.

22. Luczak, B.B., James, B.T., & Girgis, H.Z. (2019). A survey and evaluations of histogram-based statistics in alignment-free sequence comparison. *Briefings in Bioinformatics*, 20, 1222-1237.
23. Lynch, M.D., & Neufeld, J.D. (2015). Ecology and exploration of the rare biosphere. *Nature Reviews Microbiology*, 13(4), 217-229.
24. McGill, B.J., Etienne, R.S., Gray, J.S., Alonso, D., Anderson, M.J., Benecha, H.K., Dornelas, M., Enquist, B.J., Green, J.L., He, F., Hurlbert, A.H., Magurran, A.E., Marquet, P.A., Maurer, B.A., Ostling, A., Soykan, C.U., Ugland, K.I., & White, E.P. (2007). Species abundance distributions: moving beyond single prediction theories to integration within an ecological framework. *Ecology Letters*, 10, 995-1015.
25. Magurran, A.E., & Henderson, P.A. (2003). Explaining the excess of rare species in natural species abundance distributions. *Nature*, 422(6933), 714-716.
26. Magurran, A.E., & McGill, B.J. (Eds.). (2010). *Biological Diversity: Frontiers in Measurement and Assessment*. OUP Oxford.
27. Murphy, A.H. (1970). The ranked probability score and the probability score: A comparison. *Monthly Weather Review*, 98, 917-924.
28. Rijsberman, F.R. (2006). Water scarcity: fact or fiction? *Agricultural Water Management*, 80(1-3), 5-22.
29. Rousselet, G.A., Pernet, C.R., & Wilcox, R.R. (2017). Beyond differences in means: robust graphical methods to compare two groups in neuroscience. *European Journal of Neuroscience*, 46, 1738-1748.
30. Simonis, J.L., White, E.P., & Ernest, S.K.M. (2021). Evaluating probabilistic ecological forecasts. *Ecology*, 102(3), e03431.

31. Suzuki, A., Murakami, H., & Mukherjee, A. (2023). Distribution-free Phase-I scheme for location, scale and skewness shifts with an application in monitoring customers' waiting time. *Journal of Applied Statistics*, 50(4), 827-847.
32. Szeliski, R. (2022). *Computer Vision: Algorithms and Applications*. Springer Nature.
33. Tan, S., Zhang, H., Zhang, Y., Chen, W., D'Souza, W.D., & Lu, W. (2013). Predicting pathologic tumor response to chemoradiotherapy with histogram distances characterizing longitudinal changes in 18F-FDG uptake patterns. *Medical Physics*, 40(10), 101707.
34. United Nations, Food and Agriculture Organization. (2024). FAOSTAT. Crops and livestock products. <https://www.fao.org/faostat/en/#data/QCL>.
35. United States Census Bureau. (2024a). American Community Survey 1-Year Estimates: Income in the Past 12 Months (Households, Families, Individuals). <https://data.census.gov>.
36. United States Census Bureau. (2024b). American Community Survey 1-Year Estimates: Poverty Status in the Past 12 Months. U.S. Census Bureau. <https://data.census.gov>.
37. United States Department of Health and Human Services. (2024). Programs that Use the Poverty Guidelines as a Part of Eligibility Determination. <https://www.hhs.gov/answers/hhs-administrative/what-programs-use-the-poverty-guidelines/index.html>.
38. Vadyala, S.R., Betgeri, S.N., Matthews, J.C., & Matthews, E. (2022). A review of physics-based machine learning in civil engineering. *Results in Engineering*, 13, 100316.
39. Wan, Q., & Zhu, M. (2021). Detecting a shift in variance using economically designed VSI control chart with combined attribute-variable inspection. *Communications in Statistics-Simulation and Computation*, 50, 3483-3497.

40. Williams, R.F., & Doessel, D.P. (2006). Measuring inequality: tools and an illustration. *International Journal for Equity in Health*, 5, 1-8.
41. Zar, J.H. (Ed.). (2009) *Biostatistical Analysis* (5th ed.). New Jersey, USA: Prentice Hall.